

Neural Residual Flow Fields for Efficient Video Representations

Daniel Rho, Junwoo Cho, Jong Hwan Ko, Eunbyung Park
SungKyunKwan University

daniel231@skku.edu, jwcho000@g.skku.edu, jhko@skku.edu, epark@skku.edu

Abstract

Implicit neural representation (INR) has emerged as a powerful paradigm for representing signals, such as images, videos, 3D shapes, etc. Although it has shown the ability to represent fine details, its efficiency as a data representation has not been extensively studied. In INR, the data is stored in the form of parameters of a neural network and general purpose optimization algorithms do not generally exploit the spatial and temporal redundancy in signals. In this paper, we suggest a novel INR approach to representing and compressing videos by explicitly removing data redundancy. Instead of storing raw RGB colors, we propose Neural Residual Flow Fields (NRFF), using motion information across video frames and residuals that are necessary to reconstruct a video. Maintaining the motion information, which is usually smoother and less complex than the raw signals, requires far fewer parameters. Furthermore, reusing redundant pixel values further improves the network parameter efficiency. Experimental results have shown that the proposed method outperforms the baseline methods by a significant margin. The code is available in https://github.com/daniel03c1/eff_video_representation.

1. Introduction

Implicit neural representation [21, 25, 29, 32, 33] (INR, also known as coordinate-based neural representation) is a novel way of parameterizing complex signals that makes use of fully-connected neural networks. It can represent signals at any resolution, unlike other representations that save signals as discretely sampled values. Thanks to the recent breakthrough in input features, it can now accurately express both low and high frequencies of signals. Based on these advantages, it has demonstrated great potential in a variety of applications, such as computer graphics [24, 25], physical simulations [18, 29], and generative models [5, 30], to name a few.

Despite the fact that INR has recently received great attention, the network parameter efficiency of INR has not been extensively studied. In INR, it has a crucial impact on

signal transmission since signals are stored in the form of network parameters. Several recent studies have found that a model requires a large number of parameters to accurately represent signals [25, 29] and the high cost of transmission prevents INR from being used for many useful applications that would benefit from it.

In this work, we study how to efficiently represent video signals with this emerging representation. A naive approach would be to use INR as a function of spatial and time coordinates, taking continuous coordinates as inputs and producing three color channels, $(r, g, b) = f_{\theta}(x, y, t)$. There is no doubt that the universal approximator can represent this function, as evidenced by recent studies on video representation [19, 37]. However, it is not generally expected that the trained networks fully exploit the spatial and temporal redundancy of video signals to maximize the network parameter efficiency.

We propose *Neural Residual Flow Fields (NRFF)*, a novel INR scheme that leverages optical flows and residuals instead of raw colors to represent videos. Modern video compression algorithms [17, 31, 36] that leverage motion information to deduplicate signals presented across frames inspired our proposed scheme. Motion information, also known as *optical flow*, is preserved in our proposed *NRFF*, allowing similar pixel values from other frames to be reused. This alleviates the load of memorizing the same pixel values across frames and improves network parameter efficiency, as opposed to wasting network capacity on storing redundant raw signals for whole frames. However, video frames cannot be fully reconstructed using only motion information due to occlusion and dis-occlusion between frames. As a result, we also keep the *residuals* that are required to faithfully recover the original frames.

Another key motivation for our approach is that by representing motion information instead of raw color signals, the number of network parameters can be significantly reduced. Many video compression algorithms rely on block-wise motion estimations (e.g. 8×8). Each motion vector is applied to all pixels inside the block, resulting in a significant reduction in the number of motion vectors required per frame. This is based on prior knowledge that, in most

circumstances, smooth and low-frequency motion vector fields are sufficient to represent a movement between video frames. Unlike conventional discrete representations whose size is determined by the grid resolution, the required size of the implicit representation depends on signal complexity rather than volume. Given that motion vectors are less complex in general, the size of the implicit representation necessary to represent the motion vectors can be small. To reduce the total size of video representation, it is preferable to train the networks to preserve optical flows and residuals instead of more complex and generally higher-frequency raw color signals.

Experimental results show that the proposed method using flow and residuals significantly outperformed the previous baseline methods using raw colors. Under similar model size conditions, *NRFF* reconstructs video frames more clearly and sharply. On the challenging Sintel dataset [3], quantitative results show that our method improved the standard image reconstruction metrics by a large margin (improved PSNR from 30 to 37, SSIM from 0.85 to 0.95). Without any model compression techniques such as pruning, quantization, or entropy coding, the proposed method performs favorably at low bit-rates compared to the H.264 video compression algorithm [36] in both challenging synthetic and real-world videos.

2. Related Works

Implicit Neural Representations. Neural networks can be used to parameterize implicitly defined functions [29]. Since a wide variety of tasks can be represented in implicit forms, this approach has recently gained popularity and is used in several tasks, such as image [11, 21], audio [29], 3D shape [1, 24], and novel view synthesis [22, 25, 38]. Thanks to recent innovations [2, 11, 25, 29, 33], it can now effectively reconstruct fine details of signals. In addition, INR has been applied in video-related tasks [4, 9, 19]. INR has also showed promising results in novel view synthesis for videos [9, 19].

Optical Flow Estimation. Optical flow has been a core component of various computer vision tasks. Since the work of Horn and Schunck [16], many improvements have been proposed to make optical flow more accurate [12]. Recently, employing neural networks to improve optical flow estimation [7, 13, 14] rather than traditional algorithm-based methods [12] has been successful. To achieve more robust learning based optical flow methods, the ground truth optical flows have been collected by using an animated film and computer graphics [3, 7]. Several strategies have been proposed to improve estimating performance by using occlusion masks [39] or transformer-based operations [15, 34]. Although our trained model can produce fairly accurate op-

tical flow estimation, we do not aim to improve optical flow algorithms themselves by any means. We used the existing methods to guide our initial flow estimation models, which helped better reconstruction at the end.

Learning Based Video Compression. There have been several data-driven attempts to utilize neural networks for efficient video representation. Convolutional neural networks (CNN) and auto-encoder architectures have been used to compress video signals [20, 28]. These works train encoder and decoder networks on large-scale datasets and test them on unseen videos to achieve high video compression rates, assuming decoder networks are already shared and only core video information needs to be stored or sent. DVC [20] has achieved compression rates comparable to or slightly better than modern video compression algorithms, e.g., H.264 and H.265. However, these approaches are inherently vulnerable to the biases of training datasets. Recently, COIN [8], an INR-based image and video compressions, was proposed. COIN [8] is a vanilla INR method generating raw color signals. NeRV [4] used a variant of INR and achieved video compression performance comparable to that of traditional video compression algorithms. However, it takes only time coordinate t as input, thus, the model can only output images with a fixed resolution. In both methods [4, 8], there are no explicit schemes to remove temporal and spatial redundancy. On the other hand, the proposed method, *NRFF*, explicitly removes the redundancy by combining residuals and flows with the help of key frames.

3. Method

Figure 1 illustrates an overview of our proposed method. Starting from the key frame (Sec 3.4) that is located in the middle of a video sequence, we recursively apply flow (Sec 3.1) predictions from an implicit neural representation to warp (Sec 3.2) the previously reconstructed frame. Finally, the residuals are added to complete the reconstruction (Sec 3.3). We used a single MLP for estimating both optical flows and residuals.

3.1. Dense Optical Flow Estimation

The sparse motion information across frames is estimated and stored in most video compression techniques. A block with the predefined block size, such as 8×8 , is matched across frames during the encoding phase and motion vectors for each block are estimated. The main motivation for this approach is to reduce the number of motion vectors to be stored, and it is well justified because most motions in real-world signals are smooth. However, because of this algorithmic nature, many compressed videos often contain block-shaped distortions or artifacts. We propose using dense, pixel-wise motion vectors instead of block-wise mo-

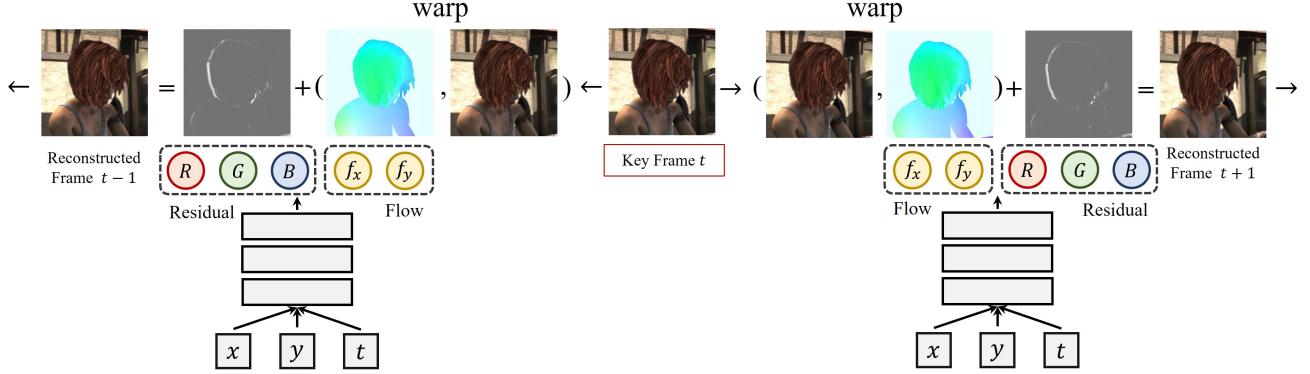


Figure 1. The proposed method is as follows: for each group of pictures, a key frame is selected in the middle. For each frame, our implicit function generates optical flows and residuals. Starting with the key frame, optical flows are applied recursively to produce warped images, which are then combined with residuals to reconstruct frames.

tion vectors. In order to reduce the spatial complexity of the dense vectors, we use a neural network to generate optical flows given spatial and temporal coordinates. It is known that representing smooth signals with the neural networks can be done efficiently [27, 33] and we can reduce the spatial complexity of the dense optical flows by constructing small size neural networks.

3.2. Image Warping

Given dense optical flows, we can easily move and reuse pixel values from other video frames. In more detail, our flow estimation network predicts a continuous dense flow field that maps pixel values in the previous frame (or future frame) to the pixels in the future frame (or previous frame). We employed a bilinear interpolation scheme to warp images in order to use continuous flow fields. Let I be an image function that takes spatial coordinates (x, y) as an input and produces corresponding colors (r, g, b) as an output. Then, a warped image $\tilde{I}^t(x, y)$ at time t from the previous frame at time $t - 1$ can be written as

$$\tilde{I}^t(x, y, t - 1) = I^{t-1}(x + \Delta x_{t-1}^t, y + \Delta y_{t-1}^t), \quad (1)$$

$$\text{where } \Delta x_{t-1}^t, \Delta y_{t-1}^t = F_{\text{flow}}(x, y, t, t - 1; \theta, \phi). \quad (2)$$

I^{t-1} can be the pixel values from the ground truth frame at time t or from the estimated frame at time t . $F_{\text{flow}}(\cdot)$ is the optical flow estimator parameterized by shared parameters θ and flow estimator specific parameters ϕ . Similarly, a warped image $\tilde{I}^t(x, y)$ from the next frame can simply be obtained as follows,

$$\tilde{I}^t(x, y, t + 1) = I^{t+1}(x + \Delta x_{t+1}^t, y + \Delta y_{t+1}^t). \quad (3)$$

3.3. Image Completion

For several reasons, reconstructing a video frame by simply warping the source video frame is likely to contain ar-

tifacts. Artifacts can be caused by a variety of factors, including imprecise optical flow estimation, occlusions and disocclusions between video frames, and accumulated errors from the recursive frame generation process. To reduce these artifacts during image warping, we propose using residuals as well as optical flows. To fully reconstruct a video frame, we add estimated residuals to the warped frame. The equation for image completion can be written as

$$\hat{I}^t(x, y) = F_{\text{res}}(x, y, t; \theta, \psi) + \begin{cases} \tilde{I}^t(x, y, t - 1), & \text{if } t > \kappa \\ \tilde{I}^t(x, y, t + 1), & \text{if } t < \kappa \end{cases} \quad (4)$$

, where F_{res} denotes the residual estimator, which has its own parameter ψ as well as a shared parameter θ with the flow estimator. κ is the index of the key frame. As equation (4) shows, we do not reconstruct a frame at time κ because we already stored the key frame information through JPEG.

3.4. Key Frames

Inspired by the standard video compression algorithms, we store a key frame per group of pictures as a standalone frame so that other frames directly or indirectly depend on the key frame. We use the JPEG image compression algorithm [35] to encode key frames. Regarding key frames, there are two important considerations: the image quality of key frames and which frames to select per group of pictures.

There is a trade-off between key frame image quality and compression ratio. In addition, we should also consider the size of the neural network, which is used for flow and residual prediction. A naive approach is to choose the highest image quality for storing key frames and a large network. It would be the best option in terms of video quality, but it would result in lower video compression rate. Given a high-quality key frame, a small neural network may suffice to achieve a certain level of video quality because the high-

frequency details in the key frame can be reused. In contrast, if a low-quality key frame is provided, a much larger network is required to generate complex high frequency signals that are omitted in the key frame. Finding the optimal combination of the network size and the key frame quality is beyond the scope of this paper and we empirically found a few combinations of JPEG image quality and network size in the experimental section.

The accumulated errors for a specific frame increase as the distance from the key frame increases due to the recursive nature of the proposed approach. Thus, we chose the middle frame as the key frame to minimize the accumulated errors caused by the distance from the key frame. Experimental results demonstrated that selecting the middle frame as the key frame is better in terms of reconstruction quality than selecting the first or last frame in the group of pictures.

We could also use another INR for the key frame representation. However, we found that existing INR training techniques underperform standard JPEG algorithms and this resulted in lower video compression rates. Advanced training algorithms, input features, and novel network architectures are needed to improve current INR’s image compression performance, which eventually allows us to use INRs for the entire algorithm.

3.5. End-to-end Training

Our proposed approach was designed to be differentiable throughout the entire process in order to build an end-to-end framework for video representation learning. We used MSE (mean squared error) loss to minimize the reconstruction errors. Let T be the number of frames and κ be the index of the key frame, then the loss function can be written as

$$L(\theta, \phi, \psi) = \frac{1}{Z} \sum_{t \in [1, T] \setminus \kappa} \sum_x \sum_y \|I^t(x, y) - \hat{I}^t(x, y)\|^2. \quad (5)$$

We multiplied the equation with the constant Z to get the average loss over both time and space. Note that we exclude the key frame during the training process. The key frame will only be included during the evaluation.

3.6. Pretraining

Despite the fact that the proposed method is fully trainable in an end-to-end fashion, we observed that starting with end-to-end training proved ineffective. When we use the equation (5) to train the flow and residual network from scratch, the network tends to squander capacity by not fully leveraging optical flows during training. The equation (5) does not prohibit the network from inefficiently reconstructing a video without fully exploiting optical flows. As a result, we use estimated optical flows and residuals from an optical flow estimation method [15] as ground truth labels to pretrain the model. This contributes to the faster con-

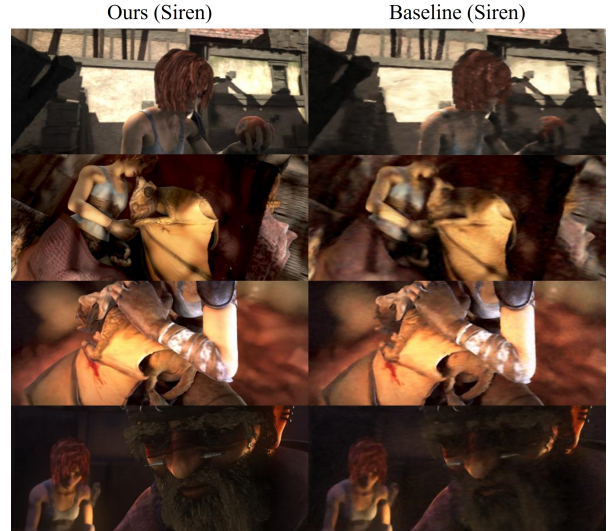


Figure 2. The qualitative results between the proposed method and the baseline method (Best viewed in color electronically).

vergence of the model. We use the equation (5) to train the model without optical flow supervision to find optimal flows and residuals for video reconstruction once the network has converged.

Another trick we have introduced is warping the ground truth frames instead of estimated frames to reconstruct video frames at an early training stage. Due to the recursive nature of our proposed method, reconstruction errors are accumulated, and this results in poor reconstruction quality even with fairly accurate flow estimations. As the frames get further away from the key frames, the problem worsens. As a result, we assign warm-up periods to reconstruct frames based on ground truth frames, prior to the end-to-end training with estimated frames. Figure 6 shows qualitative results of the trained optical flow and residual outputs with and without the suggested pretraining techniques.

4. Experiments

4.1. Dataset

We tested our approach on both synthetic and real-world datasets. We used the MPI Sintel [3] dataset as a synthetic dataset and the UVG [23] dataset as a real-world video dataset.

The MPI Sintel [3] dataset was originally designed to evaluate the optical flow performance and it provides challenging and natural video sequences based on an open source animated film. We selected the Sintel dataset for two reasons. First of all, it provides the ground truth optical flow, which allows us to evaluate the accuracy of the learned flows. Flow estimation is a core part of our algorithm, therefore, it is desirable to understand how flow estimation affects the final reconstruction. Second, it has

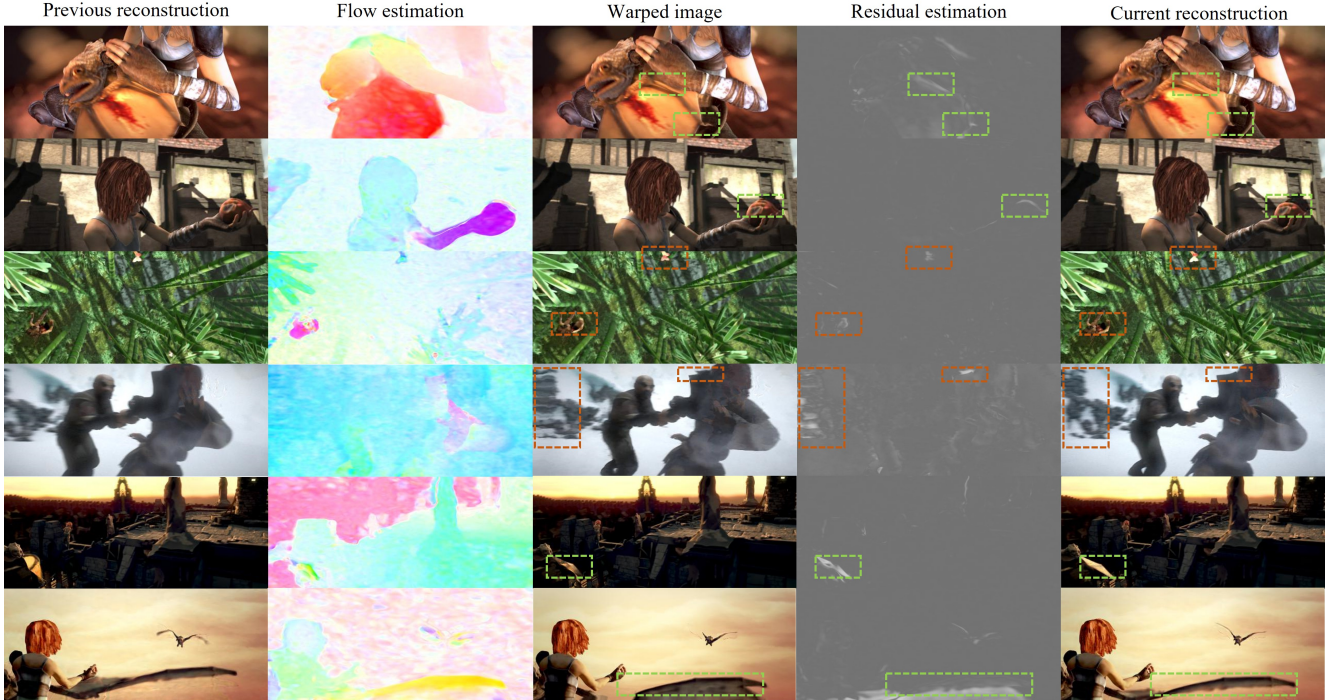


Figure 3. The qualitative results on the MPI Sintel dataset: The first column: previously reconstructed image. The second: flow estimation of our model. The third: warped images. The fourth: residual (color enhanced for better visualization). The fifth: current reconstructed images.

been a good testbed for challenging scenarios, such as long range motion, motion blur, multi-frame analysis, and non-rigid motion. They provide different levels of complexity, and we used ones that are produced with a full rendering process, which includes motion blur, camera blur, and various illumination effects. It has a total of 23 videos, and each video has about 20-50 frames. We tested our method on the entire 23 videos, and for each video, we used the first 28 frames, except for *ambush_2* and *ambush_4*, which we used the first 14 frames since those two only have less than 20 frames. We believe that good performance on this dataset would strongly support the effectiveness of the proposed method.

We also tested our method on Ultra Video Group (UVG) collection. Due to the limited computational budget, we chose six 1K resolution videos, reduced their height and width by half, and used the first 100 frames from each video. We compared our method against H.264 [36] and the baseline method, SIREN [29]. For optical flow pretraining, we used the publicly available MaskFlowNet [39] model to extract optical flows.

4.2. Experimental Setup

Network Architecture and the Key Frame Quality. We used a simple MLP architecture with 3 layers. We adjusted widths of the network to tune the model capacity,

Method	Model size (bytes)	Network width	JPEG quality
Ours	~ 100K	24	70
	100 ~ 200K	32	85
	300 ~ 500K	64	95
	700 ~ 900K	96	98
Baseline	52K	64	.
	202K	128	.
	800K	256	.

Table 1. The network capacity and corresponding key frame quality to represent 28 frames of the videos. The total model size is the sum of the network parameters and the size of the key frames. Therefore, the total size varies depending on the size of the key frames for different videos.

and the sine activation function was used. Another important consideration is choosing the right image quality for key frames. If it is of low quality, our networks will use the most capacity to recover the fine details. If it is of high quality, then it would hurt the video compression rates. We tested four different configurations in this experiment, as presented in Table 1. For baseline models, we used the same MLP architectures with varying widths to match the sizes of our models.

Training Details. We set the size of the group of pictures

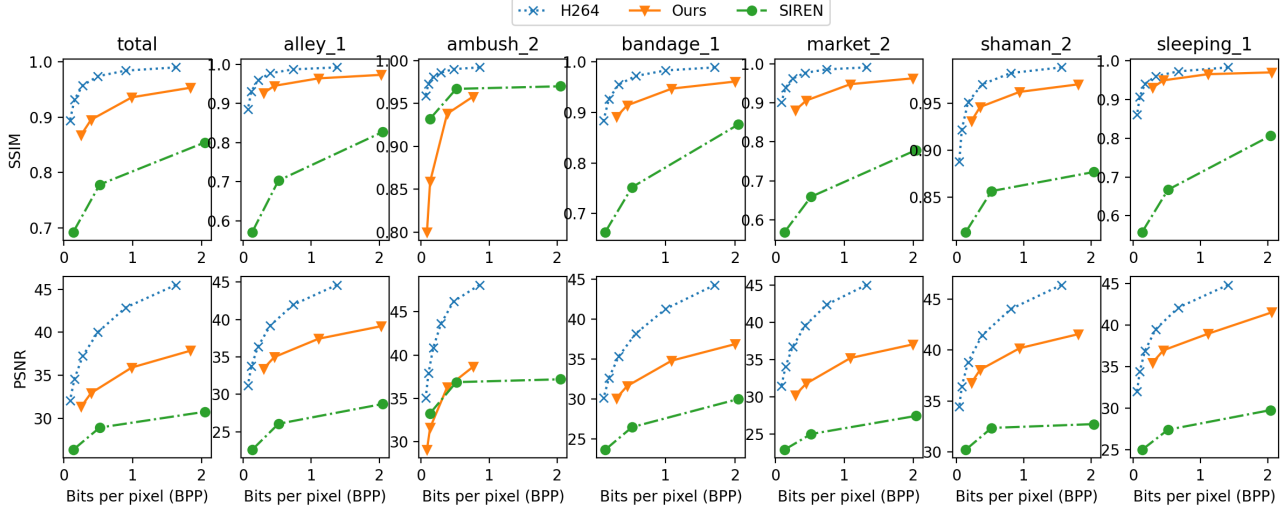


Figure 4. The quantitative results on the MPI Sintel dataset. Total means the average results of all videos in the Sintel dataset. The rest of the plots will be provided in supplementary materials.

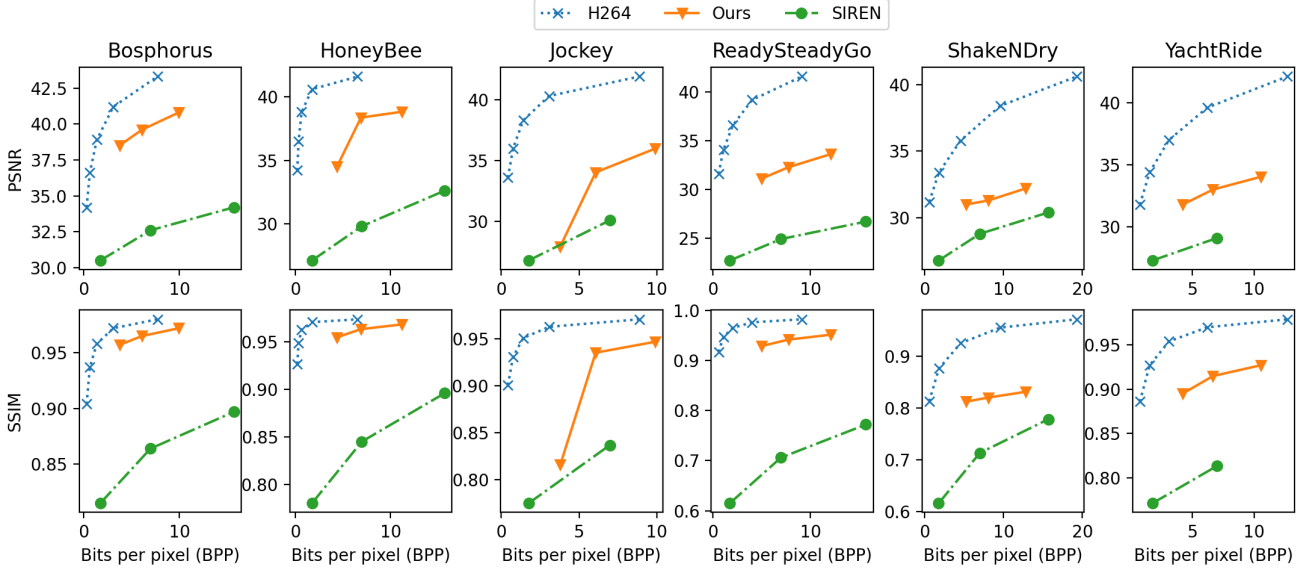


Figure 5. The quantitative results on the UVG dataset between the proposed method and the baseline method.

to seven, so that each key frame covers six neighboring frames. In the case of a video containing 28 frames, for example, we trained four models for the video.

Due to the page limits, we presented the results of five videos in the Sintel dataset. The resolution of all videos was reduced by half, resulting in 218×512 pixels. We chose the middle frame as the key frame. We trained each model for total 30K iterations, and training the whole batch of frames at once was considered a single iteration. We used the Adam optimizer with a learning rate of 0.0005. For the first 2K iterations, each model was trained with the predicted optical flows and residuals from other optical flow

models [15] as ground truth labels for flows and residuals. During the next 3K iterations, we used ground truth video frames as source images for image warping, as described in Section 3.6. To minimize the accumulated errors, it was especially crucial to warm up the networks before starting to train end-to-end. We used the widely used Pillow image library [6] in Python to control the image quality of key frames. We used RTX3090 GPUs, and it takes around 1,000 seconds to train a single model, covering seven frames including the key frame. We used PyTorch [26] deep learning library to implement the proposed method.

To train models for UVG videos, we used the Adam opti-

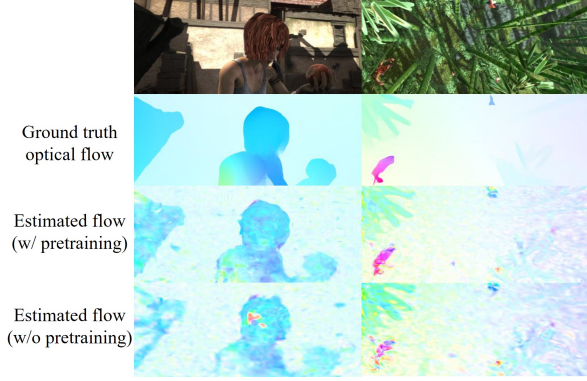


Figure 6. The impact of the proposed flow pretraining.

Video	Pretrain	MSE	PSNR	SSIM	MSE(flow)
<i>alley_1</i>	Y	0.00017	38.32	0.967	0.182
	N	0.00025	36.71	0.951	0.657
<i>bamboo_1</i>	Y	0.00068	32.49	0.940	0.128
	N	0.00075	32.12	0.935	0.177
<i>bandage_1</i>	Y	0.00042	34.82	0.940	1.325
	N	0.00054	33.88	0.923	0.923
<i>shaman_2</i>	Y	0.00008	40.83	0.968	0.098
	N	0.00009	40.57	0.968	0.135
<i>sleeping_1</i>	Y	0.00015	38.58	0.963	0.043
	N	0.00015	38.65	0.962	0.052

Table 2. Quantitative results of optical flow pretraining on the selected 5 videos.

mizer with a learning rate of $1e-5$ and a cosine decay scheduler for both SIREN and our approach. We used the first 2,500 epochs to pretrain optical flows and residuals and the next 5,000 epochs to train models using ground truth images for image warping. Similar to the Sintel dataset [3], the experimental results show that our approach outperforms the baseline method in most videos in Figure 5.

4.3. Main Results

Figure 2 illustrates the qualitative results of our method and the baseline on the MPI Sintel dataset [3]. Given similar model sizes, our strategy outperforms the baseline method by a significant margin. As illustrated in the last row of Figure 2, our method effectively preserves fine details such as a person’s beard, whereas the baseline method generates blurry outputs.

Figure 3 shows the qualitative results of our method in detail, including intermediate steps to complete video frames. The parts that need to be corrected by residuals are highlighted in figure 3. As we expected, the optical flow estimation is not necessarily accurate enough to reconstruct a frame correctly. In fact, the final optical flow estimation

includes many artifacts, particularly in the background regions. The residuals can successfully compensate for those artifacts created by inaccurate optical flows.

We also presented the quantitative results in Figure 4. We used two commonly used metrics in image reconstruction tasks; peak signal noise ratio (PSNR) and structural similarity index measure (SSIM). On average, our technique enhanced PSNR from 30 to 37 and SSIM from 0.85 to 0.95 using roughly 800KB per video. For example, in *alley_1*, we obtained 39.09 PSNR and 0.972 SSIM, as opposed to the baseline performance of 28.71 PSNR and 0.827 SSIM under similar model sizes (around 800KB). In *sleeping_1*, we got 41.56 PSNR and 0.970 SSIM, while the baseline only reached 29.78 PSNR and 0.806 SSIM. As illustrated in Figure 2, this resulted in significant increases in visual quality.

There are a few exceptions where we did not gain much improvement. One example is demonstrated in the fourth row of Figure 3. The scene is foggy and blurry, and the video shows a lot of camera movement. These factors, we believe, are the causes of the slightly lower quality of our approach. We hypothesize that, given a fixed number of parameters, inaccurate optical flow estimation may not be sufficiently compensated by residuals in some scenes. We also reported the performance of the H.264 video compression method [36] for your information. Even without any quantization, pruning, or entropy encoding techniques, our method performs well in low bit settings (low BPP), and we got near to H.264 for some videos, such as *sleeping_1*, *shaman_3*, and *mountain_1*. We believe that this is a very promising result, and we will discuss about how we can decrease the gap between conventional video compression techniques in Section 5.

In Figure 5, we also present the different results on six UVG videos [23]. As a comparison, we used H.264 [36] and SIREN [29]. When compared to the INR baseline [29] with comparable model sizes, our approach produces much cleaner and sharper videos.

4.4. Ablation Study

In this section, we report ablation studies of the suggested method. We first showed how pretraining optical flows affects reconstruction quality, and then we experimented with different activation functions to improve video quality. Finally, we analyzed the relationship between key frame location and video quality.

Optical Flow Pretraining. To examine the influence of model pretraining, we trained identical models with and without it. Figure 6 illustrates qualitative results, and Table 2 shows quantitative results. Pretrained models achieved better quality in most videos, both qualitatively and quantitatively. Their estimated optical flows were much closer to

the ground truth optical flows, and we think this is the reason for the better reconstruction quality compared to non-pretrained models. Even models that have never been pre-trained with optical flow and residual guidance can learn optical flows and residuals. As shown in Figure 6, it manages to estimate the contour of an object, e.g., the moving person, fairly accurately, but overall, estimated optical flows have some artifacts, e.g., red blobs in the person’s head. Accurate optical flow estimation may not be mandatory for achieving good reconstruction quality. However, to compensate for artifacts caused by misleading flow estimation, more parameters on residuals are usually required. As a result, the initial guidance from the optical flow supervision (in our case, it can be considered a knowledge distillation since we used a teacher optical flow model to train our model) turned out to be crucial in attaining better video quality.

Various Implicit Neural Representations. We compared two forms of implicit representation. One is SIREN [29], which uses a periodic activation function without any input feature encoding. The other is a simple MLP with non-periodic activation functions and random Fourier features. For the latter, we tested three activation functions: ReLU, LeakyReLU, and GELU [10]. The results are shown in Table 3, and "FF" in the table denotes the second form of implicit representation. GELU [10] performed best and ReLU performed worst among various non-periodic activations. However, a non-periodic activation function with random Fourier features showed much lower video quality compared to SIREN [29]. SIREN [29] showed much faster convergence rate and better quality. These results indicate that using the SIREN network architecture as a backbone was a valid strategy. We believe that searching through possible combinations of input feature encoding and activation functions might yield even better results, and we leave this for future work.

The Effects of the Key Frames. Starting with the key frame, our suggested technique uses recursive reconstruction. As a result, as the distance from the key frame increases, reconstruction errors accumulate, resulting in significantly degraded visual quality. We trained models with three different key frame locations to see how much the key frame location influences visual quality. The results are shown in Table 4. Using the middle frame as the key frame produced the best quality by a large margin, as we expected.

5. Conclusions and Discussion

We presented a way to use implicit neural representation for efficient video representation. The video quality was greatly enhanced by explicitly designing a representation model to leverage neighboring frames through flows and residuals. The proposed approach, *Neural Residual*

Method	MSE	PSNR	SSIM
SIREN	0.00017	38.32	0.967
FF-ReLU	0.00024	37.07	0.955
FF-LeakyReLU	0.00021	37.35	0.959
FF-GELU	0.00019	37.82	0.962

Table 3. Comparisons between SIREN and random Fourier features with various activation functions on *alley-1*.

Location	MSE	PSNR	SSIM
First	0.00037	33.12	0.881
Middle	0.00017	38.32	0.967
Last	0.00027	33.94	0.884

Table 4. The importance of key frame location on *alley-1*.

Flow Fields (NRFF) maintains smooth and less complex signals, which allows us to achieve more compact representations while maintaining the quality. In sum, we showed that implicit neural representation is a promising approach for video representation.

Although the results were promising, there is still room for improvement. We observed that to capture high frequency details, an implicit neural representation requires a large number of parameters and longer training iterations. It explains the wider gap between ours and state-of-the-art compression methods at high bit rates, as well as the spectral bias in training neural networks. We believe that resolving this problem would significantly enhance speed and make implicit representations more accessible in a variety of cases. Further explorations on unsupervised optical flow estimation with the implicit representations would also be an interesting research direction to improve the performance.

Note that we were able to achieve fairly good compression rates without any conventional model compression techniques. Incorporating them into our proposed method would improve the performance much further. Model quantization, weight pruning, entropy coding, and knowledge distillation could all be useful places to start.

There are a handful of promising research directions that can further make this emerging representation more attractive. We believe we have only scratched the surface, and a better understanding of the efficiency of neural network parameters in general might help answer a fundamental question about how a neural network preserves information in its parameters.

References

- [1] Matan Atzmon and Yaron Lipman. Sal: Sign agnostic learning of shapes from raw data. In *Proceedings of the IEEE/CVF Conference on Computer Vision and Pattern Recognition*, pages 2565–2574, 2020. 2
- [2] Jonathan T. Barron, Ben Mildenhall, Matthew Tancik, Peter Hedman, Ricardo Martin-Brualla, and Pratul P. Srinivasan. Mip-nerf: A multiscale representation for anti-aliasing neural radiance fields. *ICCV*, 2021. 2
- [3] D. J. Butler, J. Wulff, G. B. Stanley, and M. J. Black. A naturalistic open source movie for optical flow evaluation. In A. Fitzgibbon et al. (Eds.), editor, *European Conf. on Computer Vision (ECCV)*, Part IV, LNCS 7577, pages 611–625. Springer-Verlag, Oct. 2012. 2, 4, 7
- [4] Hao Chen, Bo He, Hanyu Wang, Yixuan Ren, Ser-Nam Lim, and Abhinav Shrivastava. Nerv: Neural representations for videos s. In *NeurIPS*, 2021. 2
- [5] Yinbo Chen, Sifei Liu, and Xiaolong Wang. Learning continuous image representation with local implicit image function. In *Proceedings of the IEEE/CVF Conference on Computer Vision and Pattern Recognition (CVPR)*, 2021. 1
- [6] Alex Clark. Pillow (pil fork) documentation, 2015. 6
- [7] Alexey Dosovitskiy, Philipp Fischer, Eddy Ilg, Philip Hausser, Caner Hazirbas, and Vladimir Golkov. FlowNet: Learning optical flow with convolutional networks. In *The IEEE Conference on Computer Vision and Pattern Recognition (CVPR)*, June 2019. 2
- [8] Emilien Dupont, Adam Goliński, Milad Alizadeh, Yee Whye Teh, and Arnaud Doucet. Coin: Compression with implicit neural representations. 2021. 2
- [9] Chen Gao, Ayush Saraf, Johannes Kopf, and Jia-Bin Huang. Dynamic view synthesis from dynamic monocular video. In *Proceedings of the IEEE International Conference on Computer Vision*, 2021. 2
- [10] Dan Hendrycks and Kevin Gimpel. Gaussian Error Linear Units (GELUs). *arXiv preprint arXiv:1606.08415*, 2016. 8
- [11] Amir Hertz, Or Perel, Raja Giryes, Olga Sorkine-Hornung, and Daniel Cohen-Or. Sape: Spatially-adaptive progressive encoding for neural optimization. In *Thirty-Fifth Conference on Neural Information Processing Systems*, 2021. 2
- [12] Berthold K. P. Horn and Brian G. Schunck. Determining optical flow. *ARTIFICIAL INTELLIGENCE*, 17:185–203, 1981. 2
- [13] Junhwa Hur and Stefan Roth. Iterative residual refinement for joint optical flow and occlusion estimation. In *CVPR*, 2019. 2
- [14] E. Ilg, N. Mayer, T. Saikia, M. Keuper, A. Dosovitskiy, and T. Brox. FlowNet 2.0: Evolution of optical flow estimation with deep networks. In *IEEE Conference on Computer Vision and Pattern Recognition (CVPR)*, Jul 2017. 2
- [15] Shihao Jiang, Dylan Campbell, Yao Lu, Hongdong Li, and Richard Hartley. Learning to estimate hidden motions with global motion aggregation. In *Proceedings of the IEEE/CVF International Conference on Computer Vision (ICCV)*, 2021. 2, 4, 6
- [16] Berthold K.P.Horn and Brian G.Schunck. Determining optical flow. *Artificial Intelligence*, 1981. 2
- [17] Didier Le Gall. Mpeg: A video compression standard for multimedia applications. *Communications of the ACM*, 34(4):46–58, 1991. 1
- [18] Zongyi Li, Nikola Kovachki, Kamyar Azizzadenesheli, Burigede Liu, Kaushik Bhattacharya, Andrew Stuart, and Anima Anandkumar. Fourier neural operator for parametric partial differential equations. In *International Conference on Learning Representations (ICLR)*, 2021. 1
- [19] Zhengqi Li, Simon Niklaus, Noah Snavely, and Oliver Wang. Neural scene flow fields for space-time view synthesis of dynamic scenes. In *Proceedings of the IEEE/CVF Conference on Computer Vision and Pattern Recognition (CVPR)*, 2021. 1, 2
- [20] Guo Lu, Wanli Ouyang, Dong Xu, Xiaoyun Zhang, Chunlei Cai, and Zhiyong Gao. Dvc: An end-to-end deep video compression framework. In *Proceedings of the IEEE/CVF Conference on Computer Vision and Pattern Recognition (CVPR)*, June 2019. 2
- [21] Julien NP Martel, David B Lindell, Connor Z Lin, Eric R Chan, Marco Monteiro, and Gordon Wetzstein. Acorn: Adaptive coordinate networks for neural scene representation. *arXiv preprint arXiv:2105.02788*, 2021. 1, 2
- [22] Ricardo Martin-Brualla, Noha Radwan, Mehdi SM Sajjadi, Jonathan T Barron, Alexey Dosovitskiy, and Daniel Duckworth. Nerf in the wild: Neural radiance fields for unconstrained photo collections. In *Proceedings of the IEEE/CVF Conference on Computer Vision and Pattern Recognition*, pages 7210–7219, 2021. 2
- [23] Alexandre Mercat, Marko Viitanen, and Jarno Vanne. Uvg dataset: 50/120fps 4k sequences for video codec analysis and development. New York, NY, USA, 2020. Association for Computing Machinery. 4, 7
- [24] Lars Mescheder, Michael Oechsle, Michael Niemeyer, Sebastian Nowozin, and Andreas Geiger. Occupancy networks: Learning 3d reconstruction in function space. In *Proceedings of the IEEE/CVF Conference on Computer Vision and Pattern Recognition*, pages 4460–4470, 2019. 1, 2
- [25] Ben Mildenhall, Pratul P. Srinivasan, Matthew Tancik, Jonathan T. Barron, Ravi Ramamoorthi, and Ren Ng. Nerf: Representing scenes as neural radiance fields for view synthesis. In *ECCV*, 2020. 1, 2
- [26] Adam Paszke, Sam Gross, Francisco Massa, Adam Lerer, James Bradbury, Gregory Chanan, Trevor Killeen, Zeming Lin, Natalia Gimelshein, Luca Antiga, Alban Desmaison, Andreas Kopf, Edward Yang, Zachary DeVito, Martin Raison, Alykhan Tejani, Sasank Chilamkurthy, Benoit Steiner, Lu Fang, Junjie Bai, and Soumith Chintala. Pytorch: An imperative style, high-performance deep learning library. In H. Wallach, H. Larochelle, A. Beygelzimer, F. d’Alché-Buc, E. Fox, and R. Garnett, editors, *Advances in Neural Information Processing Systems 32*, pages 8024–8035. Curran Associates, Inc., 2019. 6
- [27] Nasim Rahaman, Aristide Baratin, Devansh Arpit, Felix Draxler, Min Lin, Fred Hamprecht, Yoshua Bengio, and Aaron Courville. On the spectral bias of neural networks. In *International Conference on Machine Learning*, pages 5301–5310. PMLR, 2019. 3

- [28] Oren Rippel, Sanjay Nair, Carissa Lew, Steve Branson, Alexander Anderson, and Lubomir Bourdev. Learned video compression. In *2019 IEEE/CVF International Conference on Computer Vision (ICCV)*, pages 3453–3462, 2019. 2
- [29] Vincent Sitzmann, Julien Martel, Alexander Bergman, David Lindell, and Gordon Wetzstein. Implicit neural representations with periodic activation functions. *Advances in Neural Information Processing Systems*, 33, 2020. 1, 2, 5, 7, 8
- [30] Ivan Skorokhodov, Savva Ignatyev, and Mohamed Elhoseiny. Adversarial generation of continuous images. In *Proceedings of the IEEE/CVF Conference on Computer Vision and Pattern Recognition (CVPR)*, 2021. 1
- [31] Gary J. Sullivan, Jens-Rainer Ohm, Woo-Jin Han, and Thomas Wiegand. Overview of the high efficiency video coding (hevc) standard. *IEEE Transactions on Circuits and Systems for Video Technology*, 22(12):1649–1668, 2012. 1
- [32] Matthew Tancik, Ben Mildenhall, Terrance Wang, Divi Schmidt, Srinivasan Pratul P, Jonathan T. Barron, and Ren Ng. Learned initializations for optimizing coordinate-based neural representations. In *Proceedings of the IEEE/CVF Conference on Computer Vision and Pattern Recognition (CVPR)*, 2021. 1
- [33] Matthew Tancik, Pratul P Srinivasan, Ben Mildenhall, Sara Fridovich-Keil, Nithin Raghavan, Utkarsh Singhal, Ravi Ramamoorthi, Jonathan T Barron, and Ren Ng. Fourier features let networks learn high frequency functions in low dimensional domains. *arXiv preprint arXiv:2006.10739*, 2020. 1, 2, 3
- [34] Zachary Teed and Jia Deng. Raft: Recurrent all-pairs field transforms for optical flow. In *European conference on computer vision*, pages 402–419. Springer, 2020. 2
- [35] G.K. Wallace. The jpeg still picture compression standard. *IEEE Transactions on Consumer Electronics*, 38(1):xviii–xxxiv, 1992. 3
- [36] T. Wiegand, G.J. Sullivan, G. Bjontegaard, and A. Luthra. Overview of the h.264/avc video coding standard. *IEEE Transactions on Circuits and Systems for Video Technology*, 13(7):560–576, 2003. 1, 2, 5, 7
- [37] Wenqi Xian, Jia-Bin Huang, Johannes Kopf, and Changil Kim. Space-time neural irradiance fields for free-viewpoint video. In *Proceedings of the IEEE/CVF Conference on Computer Vision and Pattern Recognition (CVPR)*, pages 9421–9431, 2021. 1
- [38] Kai Zhang, Gernot Riegler, Noah Snaveley, and Vladlen Koltun. Nerf++: Analyzing and improving neural radiance fields. *arXiv preprint arXiv:2010.07492*, 2020. 2
- [39] Shengyu Zhao, Yilun Sheng, Yue Dong, Eric I-Chao Chang, and Yan Xu. Maskflownet: Asymmetric feature matching with learnable occlusion mask. In *Proceedings of the IEEE Conference on Computer Vision and Pattern Recognition (CVPR)*, 2020. 2, 5

Appendix

A. Model Details

Table 1 shows the overall structure of the representation network. "W" denotes the width of the network that controls both video quality and the network size. Only the output layers are separated for flow and residual prediction, and four layers are shared.

B. Sintel Dataset

We include the quantitative results of the Sintel dataset. The results for all 23 videos and the overall result are presented in Figure 2 and 3. Figure 4 shows additional qualitative results, including intermediate steps.

C. Training Curves

Figure 1 shows the training curve of our proposed method. We pre-trained optical flows and residuals for the first 2,000 epochs, using estimated optical flows and residuals from the optical flow estimator as ground truth labels. From 2,000 to 5,000 epochs, we trained models without flow and residual supervision. We used ground truth images

as source images for image warping throughout this period. Starting from 5,000 epochs, we trained models to reconstruct video frames without any guidance or ground truth images. Without ground truth images for image warping, errors accumulate over video frames, resulting in a significant quality drop at 5,000 epoch, after which models slowly recover.

D. Source Code

We provided a Github link for sharing our code.
https://github.com/daniel03c1/eff_video_representation.

Layer	Output Shape	Activation	Connected to
Input	(None, 3)		
Layer1	(None, W)	sine	Input
Layer2	(None, W)	sine	Layer1
Layer3	(None, W)	sine	Layer2
Layer4	(None, W)	sine	Layer3
Flows	(None, 2)		Layer4
Residuals	(None, 3)	tanh	Layer4

Table 1. Overview of the representation network

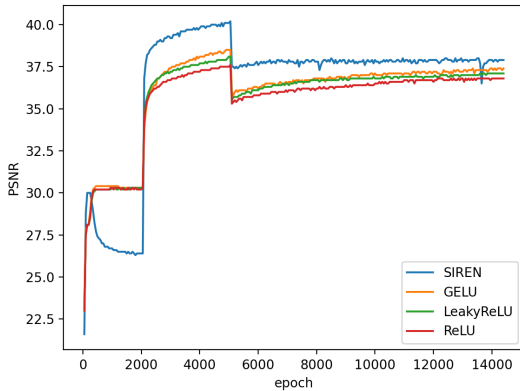


Figure 1. A training curve with different activation functions.

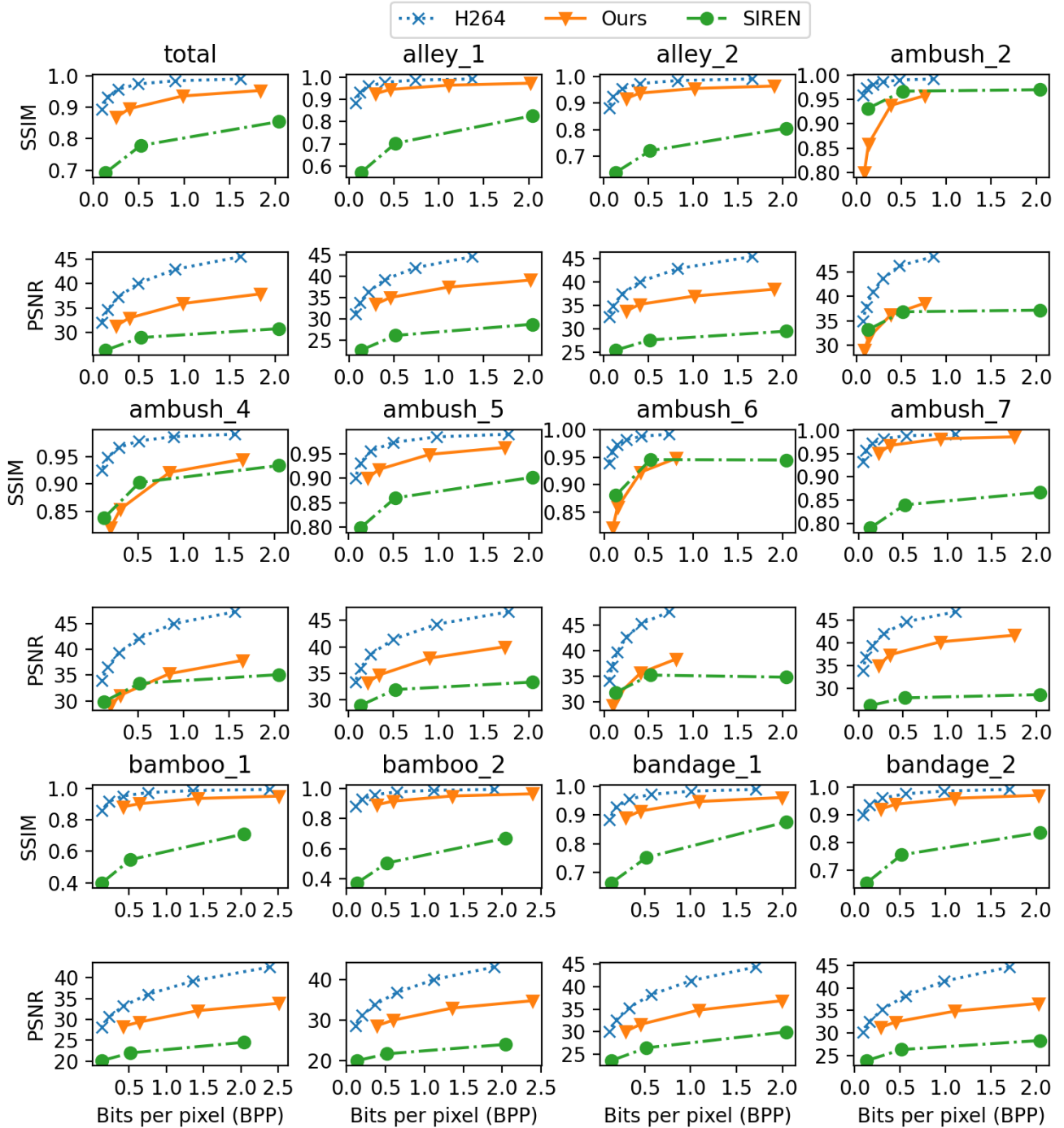


Figure 2. The quantitative results on the MPI Sintel dataset (1/2). Total means the average results of all videos in the Sintel dataset.

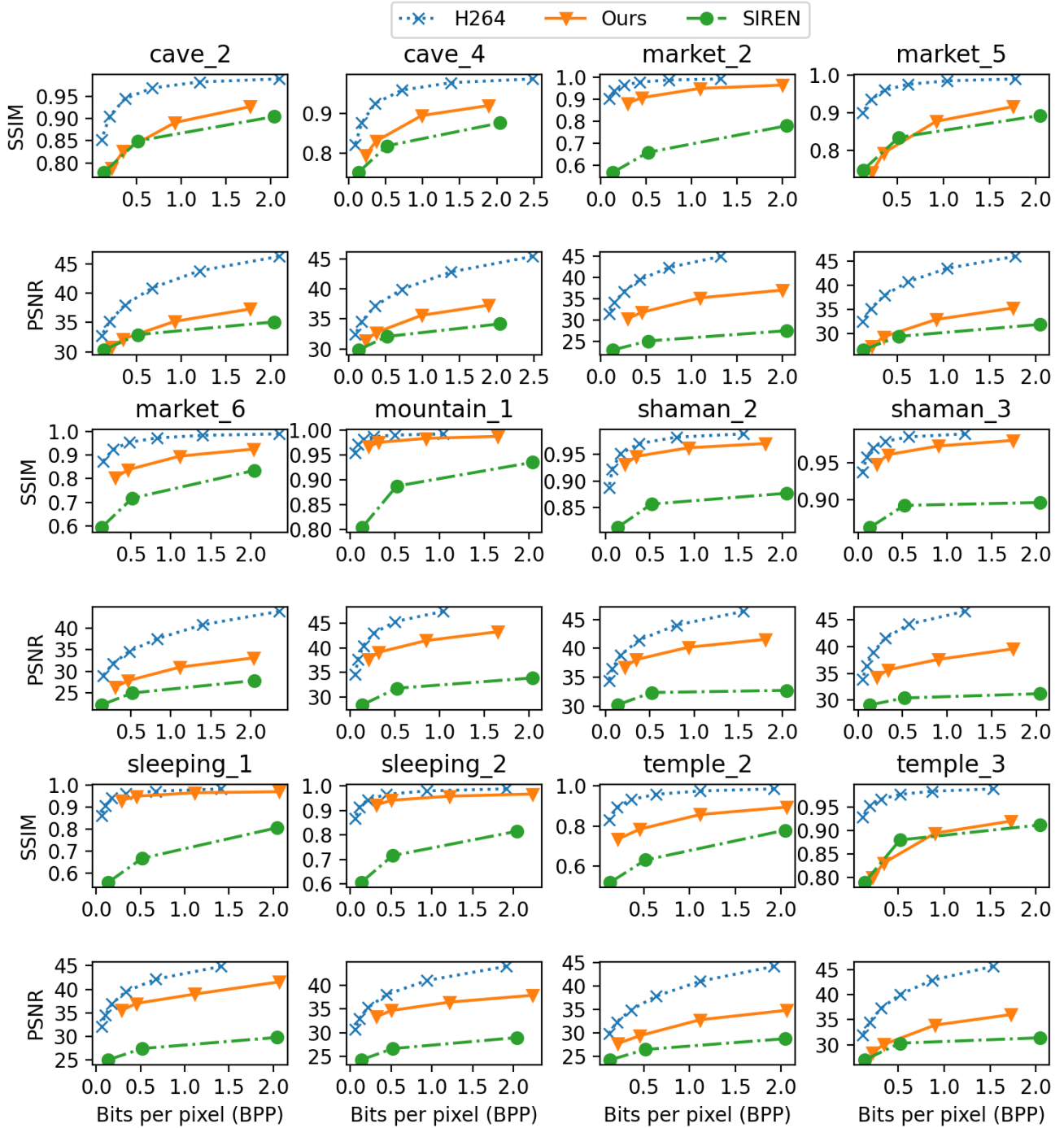


Figure 3. The quantitative results on the MPI Sintel dataset (2/2).

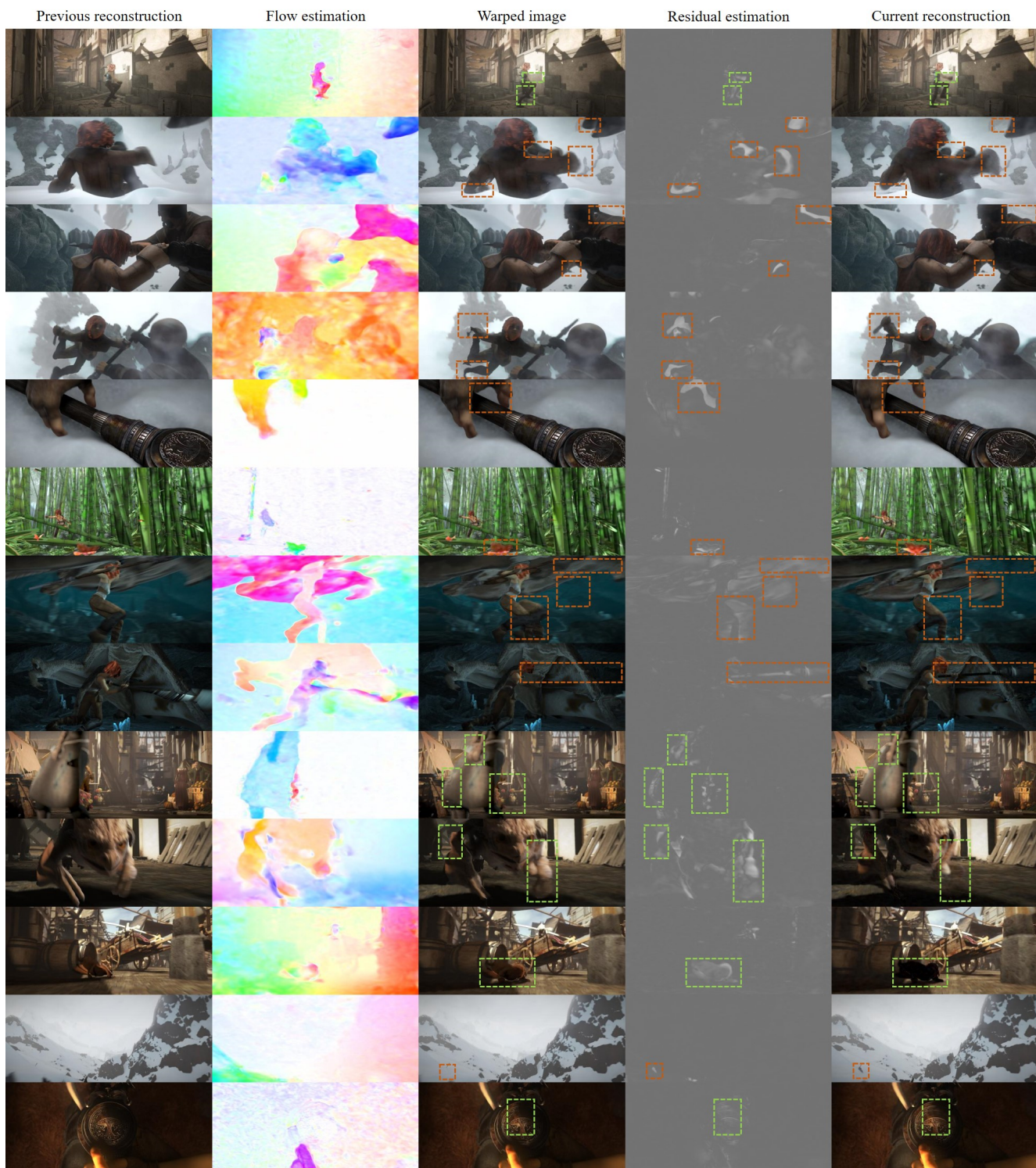


Figure 4. Additional qualitative results on the MPI Sintel dataset. The first column: previously reconstructed image. The second: flow estimation of our model. The third: warped images. The fourth: residual (color enhanced for better visualization). The fifth: current reconstructed images.